

# STUDYING SOUND PRODUCTION IN THE HOLE-TONE CONFIGURATION USING COMPRESSIBLE AND INCOMPRESSIBLE GLOBAL STABILITY ANALYSES

R.LONGOBARDI<sup>1,2</sup>, D. FABRE<sup>2</sup>, P.BONNEFIS<sup>2</sup>,  
V. CITRO<sup>1</sup>, F. GIANNETTI<sup>1</sup> & P. LUCHINI<sup>1</sup>

<sup>1</sup> DIIN; Universitá degli Studi di Salerno; Via Giovanni Paolo II, 84084 Fisciano (SA), Italy

<sup>2</sup> IMFT, Université de Toulouse, CNRS; Allée Camille Soula, 31400 Toulouse, France

## Abstract.

We study the jet passing through two successive circular holes, also known as hole-tone configuration. Such flow is relevant to many applications like human whistling, wind instruments and tea kettles.

Recently, Fabre et al. [5] investigated this flow configuration adopting a global stability approach, showing that the whistling is linked to a purely incompressible instability of the jet between the two holes. In this work, we focus our attention on a little different and more realistic geometry, known as birdcall configuration, consisting into two successive holes in curved thick plates.

Although the whistle is related to compressible phenomena, the incompressible approach can provide some useful information, at least in the region near the hole, where, in some conditions, the flow can be considered incompressible. We thus initially perform a purely incompressible stability approach. We identify the critical conditions, the global frequencies and discuss the structure of the resulting global eigenmodes. In order to reintroduce and evaluate compressible effects, which can be relevant into the cavity between the two holes, we model the cavity as a Helmholtz resonator and couple it to the incompressible simulation. Finally, a full compressible stability analysis is performed in order to check the accuracy of these simplified approaches in term of critical conditions, global frequencies and structure of the modes.

**Key words:** instability, compressible, whistle, birdcall.

## 1 Introduction

It is known that the flow passing through two circular holes in thick plates, also known as hole-tone configuration, gives rise to a whistle tone and this situation is encountered in various practical situations, such as human whistling, wind instruments or tea kettles. Such kind of problems attracted the interest of numerous acoustic researches such as Helmholtz [12], Rayleigh [16] and Bouasse [2], which investigated the problem majorly from an acoustic point of view, namely without considering the existence of a mean flow and its dynamics. More recently Henrywood & Agarwal [13] investigated the hole-tone configuration from an experimental point of view, identifying two regimes: at low velocities the whistle frequency is selected by the cavity between the two holes whereas at high speed regimes the jet

dynamics is more relevant in the frequency selection process. Recently, Fabre et al. [5] studied this problem by using an incompressible analysis thanks to the assumption of acoustically compact holes: they assumed the wavelength of the sound wave greater than the characteristic length scales of the cavity and holes. In particular, they used the global approach to compute the stability characteristics of the flow system. They found that the frequency selection is triggered by the hydrodynamic regime, although the whistle is related to compressible phenomena.

In this paper we study a more realistic geometry, namely the *birdcall configuration* (more details about the geometry are given in section 2). We investigate the whistling properties of this flow configuration using a global stability analysis. In particular, the main objectives of the paper can be summarized as follows:

- (i) Characterization of the incompressible (hydrodynamic) mechanism; we apply the classical global stability approach to the Navier–Stokes system, showing the existence of various unstable branches.
- (ii) Modeling the effect of compressibility by assuming the cavity as an Helmholtz resonator; we impose a complex spring–like impedance boundary condition on the upper wall of the cavity.
- (iii) Validation of the model by using a full compressible stability analysis.

## 2 Geometry configuration and governing equations

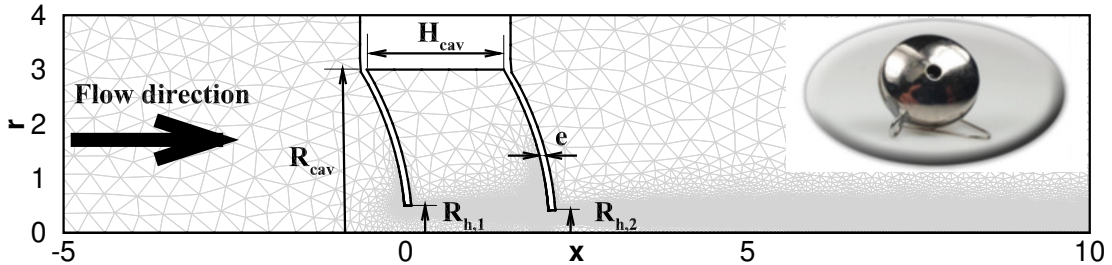


Figure 1: Sketch of the birdcall configuration, frame of reference and definition of the main geometrical parameters. An example of computational mesh is also reported in light gray. An example of the real configuration used in this paper is depicted in the upper right corner of the figure.

The birdcall configuration is a more realistic evolution of the classical hole–tone one. It consists in two successive holes in thick curved plates with the two diameters of similar dimensions. Figure 1 shows the geometry considered in this paper and an example of the mesh used for the computations. This geometry models a real whistle shown in the upper right corner of figure 1. In the actual case, the first hole is greater than the second one, whereas the thickness is considered the same for both the plates. More details about the geometrical parameters of the birdcall are reported in table 1. The birdcall connects two open spaces, whose dimensions are taken sufficiently large in order to guarantee domain size independent results. The mean flow moves from left to right driven by a pressure difference and it is

$R_{cav}$	$H_{cav}$	$R_{h,1}$	$R_{h,2}$	$e$
3	2	0.5	0.42	0.1

Table 1: Geometrical parameters of the birdcall. The labels are referred to the one reported in figure 1. All the quantities are non-dimensionalized using the diameter of the first hole.

constrained to pass through the holes, forming a recirculation region into the cavity and free shear layers into the cavity and past the second hole.

Here, we present the theoretical framework for the compressible Navier–Stokes equations: the incompressible formulation can be retrieved just taking the limit  $Ma \rightarrow 0$ . In particular, we assumed an ideal gas with a Prandtl number  $Pr = \mu c_p / \kappa$  equal to 0.7, where  $c_p$  is the constant specific heat,  $\kappa$  is the thermal conductivity and  $\mu$  is the dynamic viscosity. Moreover, we suppose that the viscosity and the thermal conductivity don't change with the temperature [18]. Under these assumptions, the compressible Navier–Stokes equations can be written as:

$$\left. \begin{aligned} \partial_t \rho + \mathbf{u} \cdot \nabla \rho + \rho \nabla \cdot \mathbf{u} &= 0 \\ \rho \partial_t \mathbf{u} + \rho \mathbf{u} \cdot \nabla \mathbf{u} + \nabla p - \frac{1}{Re} \nabla \cdot \tau(\mathbf{u}) &= \mathbf{0} \\ \rho \partial_t T + \rho \mathbf{u} \cdot \nabla T + (\gamma - 1) \rho T \nabla \cdot \mathbf{u} - \gamma(\gamma - 1) \frac{Ma^2}{Re} \tau(\mathbf{u}) : \mathbf{d}(\mathbf{u}) - \frac{\gamma}{Pr Re} \nabla^2 T &= 0 \\ \rho T - 1 - \gamma Ma^2 p &= 0 \end{aligned} \right\}, \quad (1)$$

where  $\gamma$  is the ratio of specific heats (here equal to 1.4),  $\rho$  and  $T$  are respectively the density and the temperature,  $\mathbf{d}(\mathbf{u}) = \frac{1}{2} (\nabla \mathbf{u} + \nabla \mathbf{u}^T)$  is the strain tensor and  $\tau(\mathbf{u}) = [2\mathbf{d}(\mathbf{u}) - \frac{2}{3}(\nabla \cdot \mathbf{u})\mathbf{I}]$  is the stress tensor per unit viscosity. The velocity vector is defined as  $\mathbf{u}(x, r, t) = (u_x, u_r)$  where  $x$  and  $r$  represent the axial and radial coordinates whereas  $u_x$  and  $u_r$  are respectively the axial and radial velocity components. The equations are non dimensionalized using the diameter of the first hole as length scale, the mean velocity into the first hole  $U_m$  as velocity scale and the internal density  $\rho_{in}$  and temperature  $T_{ext}$  as density and temperature references; the dimensionless pressure, following Fani et al. [8], is defined as  $\frac{p - p_{ext}}{\rho_{in} U_m^2}$ . As direct consequence of these choices, the Reynolds number  $Re$  and Mach number  $Ma$  are defined as:

$$Re = \frac{2R_{h,1}\rho_{in}U_m}{\mu} = \frac{2\dot{m}}{\mu\pi R_{h,1}}, \quad Ma = \frac{U_m}{\sqrt{\gamma RT_{ext}}}$$

where  $R$  is the ideal gas constant and  $\dot{m}$  the mass flow rate across the first hole. System (1) has to be completed by suitable boundary conditions. In particular, we assume no-slip and adiabatic conditions on the solid walls and appropriate conditions on the axis (see Fabre et. al. [6] for more details). The flow is forced to move through the holes by a pressure jump; thus, we should impose a given pressure on both inlet and outlet. Since the pressure jump is not known a priori, we prefer to impose velocity at the inlet as in Fabre et al. [6]. In particular, we impose the asymptotical Stokes solution provided by Harrison [10] with the density equal to its reference value  $\rho_{in}$ . The inlet mass flow rate is chosen in order to have a unitary mean velocity into the first hole in the incompressible case; then, we use the same

mass flow rate also for the compressible simulation. On the other side, we impose the reference value of the temperature  $T_{ext}$  and no stress boundary conditions at the outlet. In this way, the pressure jump across the two holes is automatically provided by the solution of the system (1).

### 3 Global Stability Approach

The main hypothesis of this work is that sound emissions are related to self–sustained oscillations caused by an instability of the flow. Here we use the global stability approach to shade light on this mechanism since it is largely applied in literature to explain self–sustained instabilities [3] of various flow configurations, such ad jets and wakes [4]. In order to tackle the problem, we decompose the total flow field into a steady base flow and a time harmonic perturbation, namely:

$$q(\mathbf{x}, t) = Q_B(\mathbf{x}) + \varepsilon q'(\mathbf{x}) \exp(\sigma t), \quad (2)$$

with  $\varepsilon \ll 1$ . Inserting the ansatz (2) into the Navier–Stokes equations and linearizing, we obtain two sets of PDEs; in particular, we find that the base flow is described by the steady state Navier–Stokes equations whereas the perturbation is governed by the Linearized Navier–Stokes Equations (LNSE). Imposing suitable boundary conditions to the LNSE, we are left with a generalized eigenvalue problem. The arising leading complex eigenvalue  $\sigma$  provides important information about the dynamic evolution of the system: if  $\Re(\sigma) < 0$  the system is asymptotically stable whereas  $\Re(\sigma) > 0$  indicates a system asymptotically unstable. The imaginary part of the eigenvalue, namely  $\Im(\sigma) = \omega$ , is the frequency of the global mode.

#### 3.1 Incompressible analysis

In the limit of  $Ma = 0$ , the dynamic evolution of the flow is well described by the incompressible Navier–Stokes equations. As mentioned in the introduction, one of the our aim is to use the incompressible limit ( $Ma = 0$ ) to characterize the dynamics of the birdcall. In this case, system (1) is reduced to the standard incompressible Navier–Stokes equations. As described above, introducing the flow decomposition (2) into the governing equations and linearizing, we obtain two problems. The resulting eigenvalue problem can be written as follow:

$$\left. \begin{aligned} \nabla \cdot \mathbf{u}' &= 0 \\ \sigma \mathbf{u}' + (\mathbf{U}_B \cdot \nabla) \mathbf{u}' + (\mathbf{u}' \cdot \nabla) \mathbf{U}_B + \nabla \mathbf{p}' - \frac{1}{Re} \nabla^2 \mathbf{u}' &= 0 \end{aligned} \right\}. \quad (3)$$

This system of equations is completed by imposing a zero velocity on the walls, appropriate boundary conditions on the axis [6] and free–stress boundary conditions both at inlet and outlet.

#### 3.2 Modeling the effect of compressibility of the cavity in an "augmented incompressible approach"

The aim of this section is to include the effect of the compressibility by using a simple model coupled to the incompressible equations. In particular, the main hypothesis of

this model is that the geometry is acoustically compact, namely the main geometrical parameters of the birdcall (diameter and distance between the two holes) result to be much smaller than the acoustic wavelength: under this hypothesis, in fact, we can retain that the flow is locally incompressible, leading to a constant value of the pressure inside the cavity (and also of the density since we are in the incompressible regime). If the pressure is constant, we can model the cavity as an Helmholtz resonator [1]: in this case we take into account of the compressibility effect imposing a spring-like impedance boundary condition on the upper wall of the cavity rather than a no slip one. The variation of the mass into the cavity can be written, in dimensional form, as [9]:

$$\partial_{t^d} m_{cav}^d = -\rho^d Q_{cav}^d \quad (4)$$

where  $m_{cav}^d = \rho^d V_{cav}^d$  and  $Q_{cav}^d$  are respectively the mass of the fluid inside the cavity and the flow rate outgoing from the cavity, whereas  $V_{cav}^d$  is the volume of the cavity. Note that the superscript "d" refers to dimensional quantities. For an adiabatic and isoentropic thermodynamical system, pressure and density are linked through the following relation:

$$p_{cav}^d = c_0^{d^2} \rho_{cav}^d, \quad (5)$$

where  $c_0^{d^2}$  is the speed of sound. Using the isoentropic condition (5) in equation (4), applying the non dimensionalization of the variables, and using the Fourier transform for the time derivative, the following equation is obtained:

$$\sigma p_{cav} + \frac{1}{\chi_c} Q_{cav} = 0 \quad \text{with} \quad \chi_c = V_{cav} Ma^2. \quad (6)$$

The coefficient  $\chi_c$  can be defined as a compressibility parameter and it is clear that the compressibility effects are influenced both by the Mach number and the volume of the cavity. The unknown terms  $p_{cav}$  and  $Q_{cav}$  are the augmented variables and they are linked with the incompressible unknown terms through:

$$\left. \begin{aligned} p_{cav} &= \frac{1}{S_{cav}} \int_{S_{cav}} p' dS \\ Q_{cav} &= \int_{S_{cav}} \mathbf{u}' \cdot \mathbf{n} dS \end{aligned} \right\}, \quad (7)$$

where  $S_{cav}$  is the surface of the upper wall of the cavity. Coupling the equations (6) and (7) with the incompressible linearized Navier–Stokes system (3), a generalized eigenvalue problem is obtained: its solution provides information about the stability of the augmented system with the modeled compressibility.

### 3.3 Full compressible approach

We also use the full compressible stability analysis in order to check the accuracy of the results obtained with the two previously described approaches. The system of

equations governing the stability of the compressible flow reads as:

$$\left. \begin{aligned} \sigma\rho' + \mathbf{U}_B \cdot \nabla\rho' + \mathbf{u}' \cdot \nabla\rho_B + \rho_B \nabla \cdot \mathbf{u}' + \rho' \nabla \cdot \mathbf{U}_B &= 0 \\ \sigma\rho_B \mathbf{u}' + \rho' \mathbf{U}_B \cdot \nabla \mathbf{U}_B + \rho_B \mathbf{u}' \cdot \nabla \mathbf{U}_B + \rho_B \mathbf{U}_B \cdot \nabla \mathbf{u}' + \nabla p' - \frac{1}{Re} \nabla \cdot \tau(\mathbf{u}') &= \mathbf{0} \\ \sigma\rho_B T' + \rho' \mathbf{U}_B \cdot \nabla T_B + \rho_B \mathbf{u}' \cdot \nabla T_B + \rho_B \mathbf{U}_B \cdot \nabla T' + &+ \\ + (\gamma - 1) (\rho' T_B \nabla \cdot \mathbf{U}_B + \rho_B T' \nabla \cdot \mathbf{U}_B + \rho_B T_B \nabla \cdot \mathbf{u}') &+ \\ -\gamma(\gamma - 1) \frac{Ma^2}{Re} [\tau(\mathbf{u}') : \mathbf{d}(\mathbf{U}_B) + \tau(\mathbf{U}_B) : \mathbf{d}(\mathbf{u}')] - \frac{\gamma}{Pr Re} \nabla^2 T' &= 0 \\ \rho' T_B + \rho_B T' - 1 - \gamma Ma^2 p' &= 0 \end{aligned} \right\}. \quad (8)$$

## 4 Numerical methods

We use the finite element method implemented in the open source code FreeFem++ [11] (<http://www.freefem.org/>) in order to solve the various problems of this paper. The unknown terms have been discretized using a triangular unstructured mesh, generated by the built-in Bamg routine. We use classical Taylor–Hood elements ( $P2 - P2 - P1$ ) for the incompressible equations. On the other hand, in the compressible case, we adopt  $P2$  elements for the velocity and  $P1$  for the other variables, namely pressure, density and temperature. After having obtained the variational formulations of the various problems, matrices of the arising discrete systems have been assembled by FreeFem++ libraries. The nonlinear equations for the base flow have been solved using a classical Newton method: at each iterative step the matrix inversion has been performed using the parallel MUMPS library. As far as the stability problems are concerned, we first use ARPACK library in order to localize the eigenvalues in the complex plain; then, the leading ones have been followed using the inverse iteration algorithm in order to have cheapest computations. In the compressible computation, in order to avoid the unphysical reflections of the acoustic waves from the inflow and outflow boundaries, we use a sponge zone technique combined with a grid stretching in order to assorbe and dissipate the acoustic waves (for more details see Rowley et al. [17]).

## 5 Results

### 5.1 Incompressible results

In this section, we report results obtained in the incompressible regime. In particular, figure 2 shows the growth rates and the frequencies of the most unstable eigenvalues as function of the Reynolds number. We find the existence of four unstable branches quantized in frequency, which is almost constant with the Reynolds number. At low Reynolds numbers, the dynamic is driven by the first branch ( $B1$ ), with a frequency of  $\omega \approx 3.3$ ; as the Reynolds number increases, the growth rates of the second ( $B2$ ) and then with the third ( $B3$ ) branch become dominant with frequencies respectively of  $\omega \approx 5.5$  and  $\omega \approx 7.7$ . The fourth unstable branch ( $B4$ ), on the other hand, is characterized by a frequency of  $\omega \approx 10.2$ , and never becomes dominant in term of the growth rate respect to the other ones, almost in the range

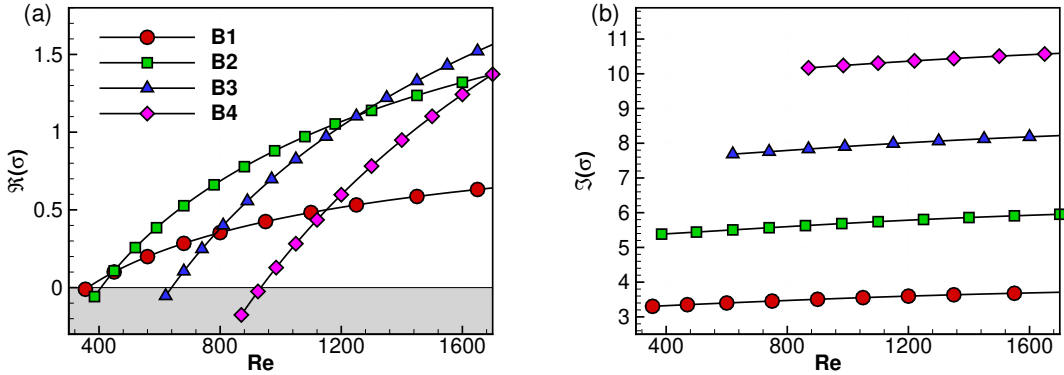


Figure 2: (a) Growth Rate and (b) frequency of the most unstable modes as function of  $Re$ . The stable region, namely  $\Re(\sigma) < 0$  is filled in gray.

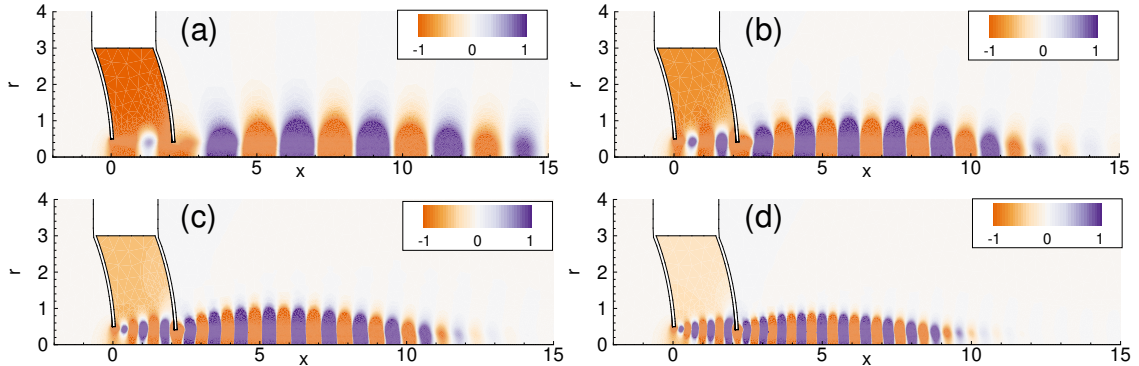


Figure 3: Real part of the pressure ( $\Re(p')$ ) for the four unstable branches at the critical Reynolds number: (a)  $Re = 363$ ,  $\omega \approx 3.3$ ; (b)  $Re = 406$ ,  $\omega \approx 5.4$ ; (c)  $Re = 639$ ,  $\omega \approx 7.7$ ; (d)  $Re = 934$ ,  $\omega \approx 10.2$ .

of Reynolds numbers investigated. Figure 3 depicts the structure of the pressure for the four unstable branches at their critical Reynolds numbers. First, it is possible to observe that at low frequencies the spatial structure of the global modes extends for a longer distance from the birdcall. Secondly, the four different unstable branches are characterized by very different structures between the two holes. The first branch is characterized by one pressure node between the two holes, the second one by two pressure nodes and so on: this means that there is a direct link between the frequency quantization and the pressure oscillations between the two holes [14].

## 5.2 Effect of compressibility

Once characterized the incompressible dynamics, we investigate the effect of the compressibility of the flow. In particular, we compare the full compressible results with the one obtained using the Helmholtz resonator augmented model described in section 3.2, in order to validate it and discuss its range of validity. Figure 4 depicts the growth rates and the frequencies obtained using the augmented model and the

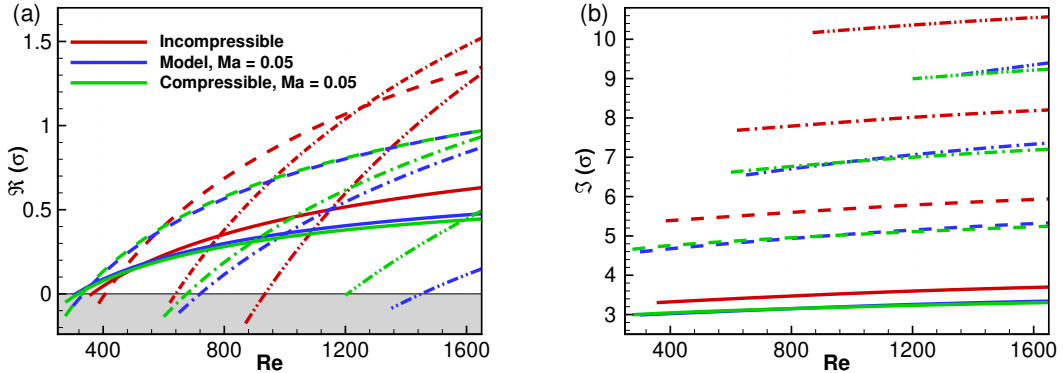


Figure 4: (a) Growth Rate and (b) frequency of the most unstable modes as function of  $Re$ . The red lines are the incompressible results, the blue lines are the model’s results whereas the green lines are the full compressible results, both computed at  $Ma = 0.05$ . The first branch  $B_1$  is reported with full lines, the second branch  $B_2$  with dashed lines, the third branch  $B_3$  with dash–dot lines and the fourth branch  $B_4$  with dash–double dot lines. The stable region, namely  $\Re(\sigma) < 0$  is filled in gray.

full compressible approach at  $Ma = 0.05$ , within the incompressible results: even if the Mach number is very low, the compressibility seems to have a considerable effect on such kind of flow configuration, as already observed by Yamouni et al. [18]. In particular, we can see that compressibility has a destabilizing effect on the first two unstable branches, in opposition to what happens in the compressible wakes [15]. Moreover, compressible effects tends to reduce the frequency of the unstable modes and this effect is as strong as the frequency gets larger. As can be noted from numerical results, the model well predicts both the growth rates and the frequencies of the unstable modes for the lower branches, namely the branch  $B_1$  and  $B_2$ , whereas it gives less accurate results for the higher ones. In figure 5 we report the comparison between the model and compressible results at  $Ma = 0.1$ . We can observe that we don’t find any unstable eigenvalues belonging to the branch  $B_1$ , almost in the range of Reynolds number investigated. Moreover, as far as the other branches goes, it easy to note that the model is not able to predict the results of the full compressible simulations.

The prediction capability of the model is strictly related to the acoustic wavelength:

$$\lambda_{ac} = \frac{2\pi}{\omega} \frac{1}{Ma}. \quad (9)$$

In fact, the main hypothesis of the model is the local incompressibility of the flow, meaning that the acoustic wavelength must be greater than the characteristic length-scale of the considered geometry. However, from equation (9) it is easy to verify that the acoustic wavelength decreases when the Mach number and the frequency increase and this explains why the model fails at high frequencies and larger Mach numbers. For the geometry considered in this paper, the greater characteristic lengthscale is the diameter of the cavity, namely  $D_{cav} = 2R_{cav}$  (see figure 1 and table 1). Numerical simulations confirm that the model is able to provide accurate results until  $\lambda_{ac} > 2D_{cav} = 12$  for the geometry considered here: if such relation does

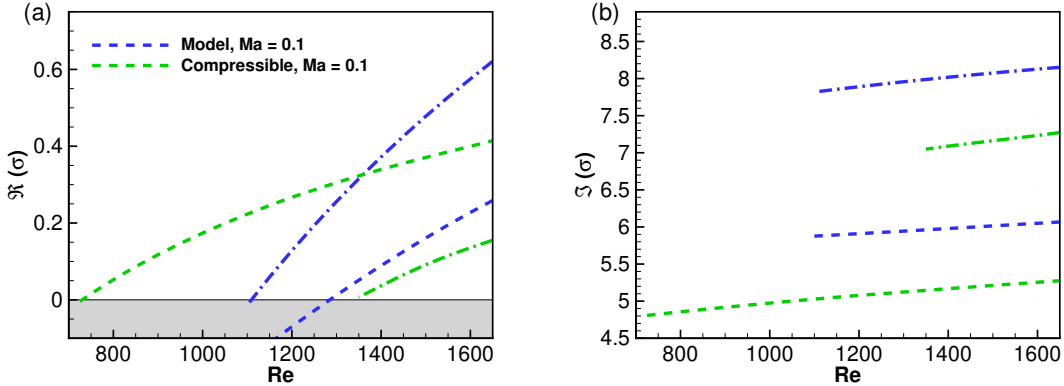


Figure 5: Same of figure 4 but for  $Ma = 0.1$ . In these figures we omit the incompressible results.

not hold, the acoustic waves are able to penetrate into the cavity and the pressure cannot be considered constant anymore contradicting the hypothesis of the model.

Finally, in figure 6, we depict the real part of the pressure of the global modes computed using the compressible equations. In particular, in figure 6(a) we report  $\Re(p')$  for  $Re = 800$ ,  $Ma = 0.05$  and  $\omega \approx 4.95$ , a case where the model returns good results, as it is possible to verify from figure 4. In particular, it is possible to observe that the acoustic waves, propagating into the far field as spherical waves, have a wavelength equal to  $\lambda_{ac} \approx 25$ , so that the relation of validity of the model is respected. In figure 6(a) it is also shown the zoom of the near field, with a different color scale, showing the same pressure patterns already observed for the incompressible mode and a constant pressure into the cavity. In figure 6(b), instead, we report  $\Re(p')$  for  $Re = 1400$ ,  $Ma = 0.1$  and  $\omega \approx 7.1$ . In this case, the acoustic wavelength is equal to  $\lambda_{ac} \approx 8.85$  and the model is outside its range of validity, as it is possible to verify from figure 5. Here, we can observe that pressure is not constant anymore into the cavity. Moreover, also the acoustic directivity seems to change when the acoustic wave is able to penetrate into the cavity, as largely reviewed by Yamouni et al. [18].

### 5.3 An example of practical application

In this last paragraph we try to set up a real experiment, that is the next step of our research. In the previous paragraph, we varied both the Reynolds and the Mach numbers independently, in order to test the augmented model and define its range of validity. Actually, if we want to simulate a real situation, this is not true, since the Reynolds and Mach numbers result to be linked, as shown by Fabre et al. [7]. In particular, the Mach number results to be proportional to the Reynolds number:

$$Ma = \frac{U_m^d}{c_0^d} = \underbrace{\frac{\nu^d}{D_{h,1}^d c_0^d}}_{K_p} Re. \quad (10)$$

In order to simulate the experiment, we use the measures of a real birdcall depicted in the upper right corner of figure 1. In particular, the dimensional diameter of

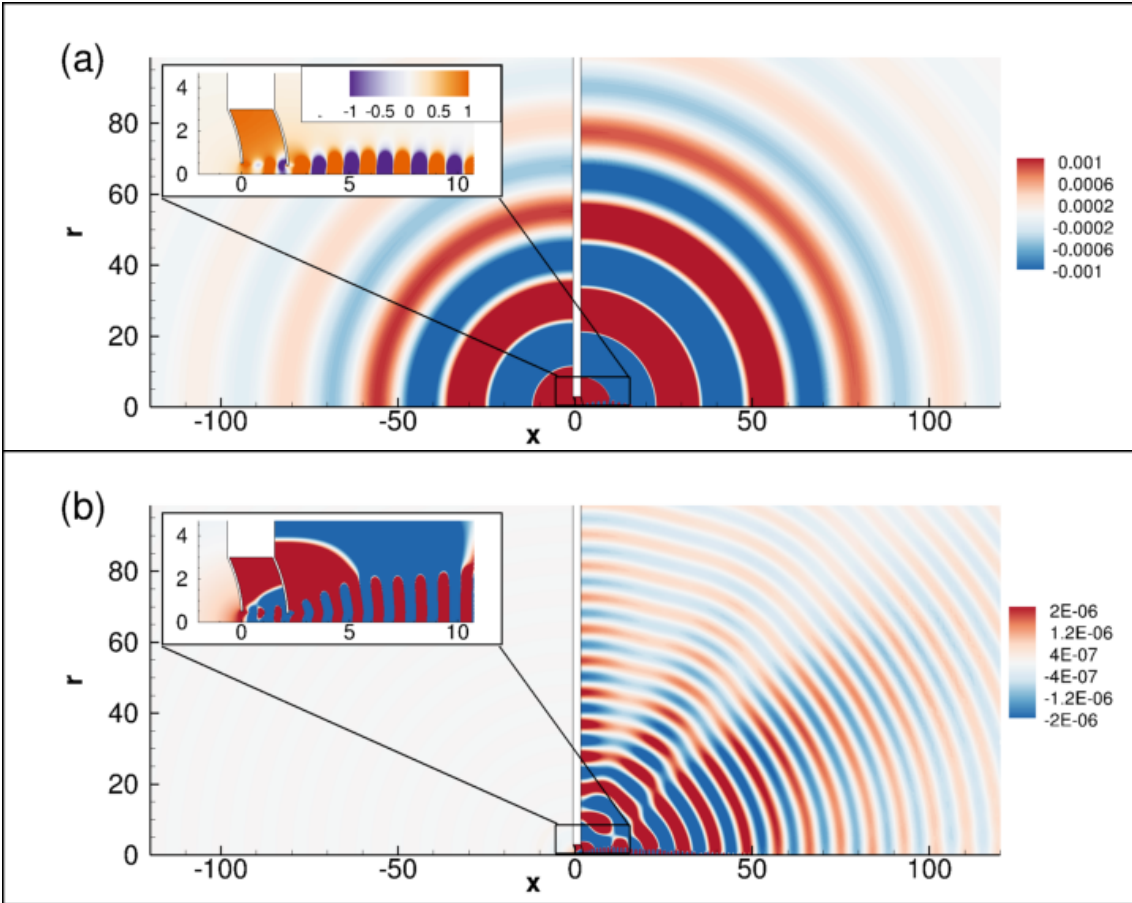


Figure 6: Real part of the pressure global modes  $\Re(p')$  for: (a)  $Re = 800$ ,  $Ma = 0.05$  and  $\omega \approx 4.95$ ; (b)  $Re = 1400$ ,  $Ma = 0.1$  and  $\omega \approx 7.1$

the first hole results to be equal to  $D_{h,1}^d = 3\text{mm}$  whereas the air temperature is hypothesized to be  $T^d = 300K$ : the other properties of the air have been obtained from a standard table, leading to a value of  $K_p \approx 1.5 \cdot 10^{-5}$ . The range of Reynolds number investigated here is  $Re \in [300 - 1650]$  leading to a range of Mach number  $Ma \in [0.004 - 0.025]$ . The use of the model rather than the full compressible simulation is here justified, at least for this specific geometry, by three main statements: first, the higher Mach number is small enough to have a good accuracy of the model, as demonstrated in the previous section; secondly, the full compressible simulation at very low Mach numbers can result very expansive since the acoustic wavelength grows, requiring very big domains with very long sponge zones; finally, the model has a very fast computation respect to the full compressible case, since we don't need sponge regions.

In figure 7 we report the comparison between the incompressible results and the one obtained with the augmented model. One can note that for the first two lower branches results are very slowly affected by compressibility, both in term of growth rate and frequency and the incompressible approximation is able to give good results. On the other hand, the effects of the compressibility are larger for the branches three and four. However, for all the unstable branches, we can observe two common features: (1) the compressibility has a destabilizing effect for this flow configura-

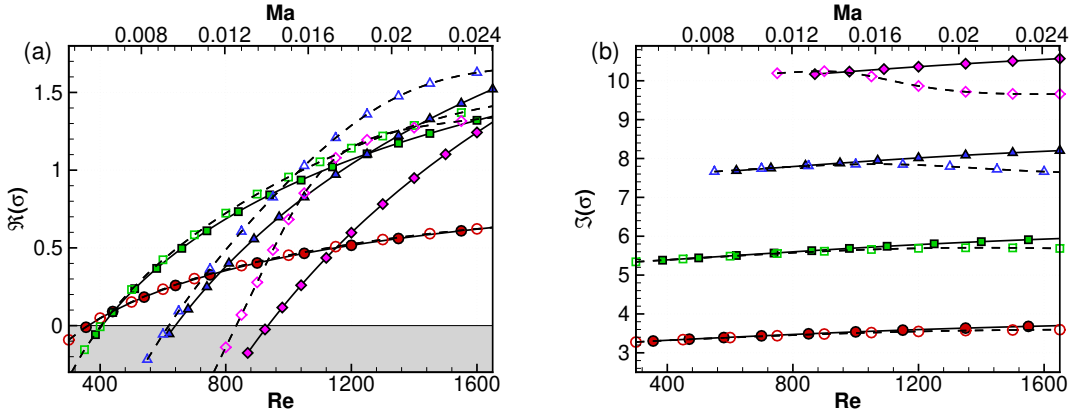


Figure 7: (a) Growth Rate and (b) frequency of the most unstable modes as function of  $Re$  and  $Ma$ . The legend is the same of figure 2: the full symbols with solid lines are the incompressible results whereas the empty symbols connected by dashed lines are the compressible augmented ones. The stable region, namely  $\Re(\sigma) < 0$  is filled in gray.

tion; (2) the frequency is usually smaller than it is in the incompressible case. This effect is more enhanced when the Reynolds (and consequently the Mach number) increases.

## 6 Conclusions

In this paper we investigate the whistling properties of a birdcall using the global stability approach. In particular, we first use a full incompressible approach in order to characterize the dynamic of such kind of flow configuration. We find four unstable branches which are quantized in frequency. The associate pressure field of the leading global modes shows pressure oscillations between the two holes and such pattern is conserved along each branch: in fact the first branch has only one pressure node, the second one is characterized by two pressure nodes and so on.

Once the incompressible dynamic has been characterized, we have considered the effect of the flow compressibility. In particular, we have first modeled the cavity between the two holes as an Helmholtz resonator. Then, we have performed a full compressible stability analysis in order to test the model and figure out the range of validity of both the incompressible approximation and the augmented model. We have found that the compressibility has an important effect on the stability of such kind of system, in term of both growth rate and frequency: in general, the compressibility reduces the frequency of the global modes, for almost all low Mach numbers investigated.

Numerical results have shown that the model is able to give accurate results only when the acoustic wavelength is greater than two cavity diameters, namely  $\lambda_{ac} > 2D_{cav}$ , almost for the configuration investigated in this paper.

The last part of the paper, finally, is about a practical application: in fact we have simulated a real experiment, in which the Reynolds and Mach number are proportional through a parameter that is function of the real geometry and air conditions. We have considered the effect of the compressibility using the model

since the relation of validity is respected. We have found that, in a real experiment, the incompressible approximation gives good results for low Reynolds (and Mach) numbers and low frequencies, whereas the effect of compressibility is relevant at higher frequencies and Reynolds (and Mach) numbers.

## References

- [1] P. Bonnefis. Etude theorique et numerique d'un jet sifflant. Master's thesis, IMFT, 2014.
- [2] H. Bouasse. *Instruments à vent*. Impr. Delagrave, 1929.
- [3] V. Citro, F. Giannetti, and J.O. Pralits. Three-dimensional stability, receptivity and sensitivity of non-newtonian flows inside open cavities. *Fluid Dynamics Research*, 47(1):015503, 2014.
- [4] V. Citro, J. Tchoufag, D. Fabre, F. Giannetti, and P. Luchini. Linear stability and weakly nonlinear analysis of the flow past rotating spheres. *Journal of Fluid Mechanics*, 807:62–86, 2016.
- [5] D. Fabre, P. Bonnefisa, F. Charru, S. Russo, V. Citro, F. Giannetti, and P. Luchini. Application of global stability approaches to whistling jets and wind instruments. In *Proc. ISMA*, 2014.
- [6] D. Fabre, R. Longobardi, P. Bonnefis, and P. Luchini. The acoustic impedance of a laminar viscous jet through a thin circular aperture. *Journal of Fluid Mechanics*, Under review.
- [7] D. Fabre, S. Marragou, R. Longobardi, D. Lo Jacono, P. Bonnefis, B. Fry, V. Citro, F. Giannetti, and P. Luchini. The whistling jet instability: Experimental investigation and global stability modelling of a bird- call. Ercoftac Sig. 33, La certosa di Pontignano (Siena), 19–21/06/2017.
- [8] A. Fani, V. Citro, F. Giannetti, and F. Auteri. Computation of the bluff-body sound generation by a self-consistent mean flow formulation. *Physics of Fluids*, 30(3):036102, 2018.
- [9] B. Fry. Etude theorique, numerique et experimentale d'un jet sifflant. Master's thesis, IMFT, UPMC, 2016.
- [10] W.J. Harrison. The pressure in a viscous liquid moving through a channel with diverging boundaries. In *Proc Cambridge Phil Soc*, volume 19, pages 307–312, 1919.
- [11] F. Hecht. New development in freefem++. *J. Numer. Math.*, 20(3-4):251–265, 2012.
- [12] H. Helmholtz. The theory of sound. *Nature*, 17(430):237, 1878.
- [13] R.H. Henrywood and A. Agarwal. The aeroacoustics of a steam kettle. *Physics of fluids*, 25(10):107101, 2013.
- [14] K. Matsuura and M. Nakano. A throttling mechanism sustaining a hole tone feedback system at very low mach numbers. *Journal of Fluid Mechanics*, 710:569–605, 2012.
- [15] P. Meliga, D. Sipp, and J.M. Chomaz. Effect of compressibility on the global stability of axisymmetric wake flows. *Journal of Fluid Mechanics*, 660:499–526, 2010.
- [16] Lord Rayleigh. The theory of sound, 1945.
- [17] C.W. Rowley, T. Colonius, and A.J. Basu. On self-sustained oscillations in two-dimensional compressible flow over rectangular cavities. *Journal of Fluid Mechanics*, 455:315–346, 2002.
- [18] S. Yamouni, D. Sipp, and L. Jacquin. Interaction between feedback aeroacoustic and acoustic resonance mechanisms in a cavity flow: a global stability analysis. *Journal of Fluid Mechanics*, 717:134–165, 2013.